Morphological characterization and electrochemical behavior of Mg alloys in NaCl 0.1 mol/L

Flávio de Souza Costa[a], Sviatlana Lamaka[b], Hercílio Gomes de Melo[c]

Abstract

Magnesium alloys exhibit a combination of low density and high strength/weight ratio making them interesting for applications where low weight and good mechanical resistance are required. As an example of such applications, it might be cited their use in medical implants for bone healing. An alloy that contains Mg and Ca (MgCa) in its composition is a good alternative to Al-rich alloys and its corrosion behavior is investigated in this work and compared with the AZ91 alloy. Immersion tests in a solution of NaCl 0.1 mol/L for 30 min were carried out to evaluate the corrosion behavior of the main constituents of both alloys. Scanning electron microscopy (SEM) images with energy dispersive X-ray spectroscopy (EDS) analysis were used to determine the composition of the constituent phases before and after these immersion tests. The corrosion behavior of both alloys were analyzed by electrochemical impedance spectroscopy (EIS) during 24 h in NaCl 0.1 mol/L. Polarization tests after the stabilization of the open circuit potential (OCP) and after 24 h in NaCl 0.1 mol/L were also made to evaluate the corrosion rates. The polarization curves showed a higher value of current density for the MgCa alloy in NaCl 0.1 mol/L compared to that of the AZ91 alloy, for both immersion times.

Keywords: Corrosion, EIS, Magnesium alloys, MgCa, AZ91.

Introduction

Metallic implants in the human body suffer a major challenge from stress shielding, reducing their service life, and, eventually, requiring surgical replacement. Stress shielding is the inhomogeneous transfer of stress between the implant and the bone, and it can cause bone resorption, hindrance to the healing process and implant loosening (Chen *et al.* (1)). Therefore, intensive efforts are directed in recent years to the development of biodegradable implants. These are non-toxic implant materials that are resorbed by the human body after a certain period of time.

Magnesium and its alloys appear to be among the best candidates for the production of biodegradable metallic implants due to their biocompatibility and excellent mechanical properties. Indeed, a substantial amount of Mg is taken into the human body daily and it is beneficial for bone strength and growth, also stimulating the metabolism as cofactor for certain enzymes. Further, any excess Mg is harmlessly excreted with the urine. The major drawback in the use of Mg alloys as implants is their tendency to corrode very fast in chloride solutions, including physiological media (which has a pH of 7.4 to 7.6), thereby losing their mechanical integrity before the expected service life. Despite these limitations, Mg alloys can still be used as biodegradable temporary implant devices such as plates, wires, stents, pins, and screws.

[a]Master, PhD student at Universidade de São Paulo
[b]PhD, Researcher at Helmholtz-Zentrum Geesthacht, Geesthacht, Germany
[c]PhD, Professor at Universidade de São Paulo

In fact, in such use, the susceptibility of Mg to rapid electrochemical dissolution can be exploited. Since Mg can dissolve and corrode away in the chloride-containing aqueous solutions (such as the physiological medium), it may be possible to obviate the need for second surgery (Choudhary *et al.* (2)). The overall corrosion reaction of Mg in aqueous environments is given below (Witte *et al.* (3)):

$Mg_{(s)} + 2H_2O_{(aq)} \rightleftharpoons Mg(OH)_{2\,(s)} + H_{2\,(g)}$ (1)

It may include the following partial reactions:

$Mg_{(s)} \rightleftharpoons Mg^{2+}_{(aq)} + 2e^-$ (anodic reaction) (2)
$2H_2O_{(aq)} + 2\,e^- \rightleftharpoons H_{2(g)} + 2OH^-_{(aq)}$ (cathodic reaction) (3)
$Mg^{2+}_{(aq)} + 2OH^-_{(aq)} \rightleftharpoons Mg(OH)_{2(s)}$ (product formation) (4)

Compared to high purity magnesium none of the alloying elements improve the corrosion behavior of Mg alloys. Al is toxicological and can cause muscle fiber damage, mild foreign body reactions and poses a risk factor in generation of Alzheimer's disease. On the other hand, Zn is neurotoxic at higher concentrations (Witte *et al.* (3)).
In this work a Mg alloy containing calcium (MgCa) and the AZ91 Mg alloy were compared for their corrosion behavior by means of electrochemical tests and microstructural characterization.

Materials and Methods

The chemical composition of the AZ91 alloy was assessed by Inductively Coupled Plasma Optical Emission Spectrometry (ICP-OES, Ultima 2, Horiba Jobin Yvon). A SPECTROLAB Spark Discharge Optical Emission Spectroscopy (SD-OES) device with Spark Analyser Vision^{TM} software was used to determine the elemental compositions of MgCa alloy. All the measurements were repeated at least two times on two different samples. The average values are presented in Table 1. For some elements, like Ca, SD-OES measurements are not reliable because of the signal overlap with that of other elements. In that case, Atomic Absorption Spectroscopy (AAS) was used from Agilent Technologies 240FS, λ=422.7 nm.
In order to perform the electrochemical essays and to obtain Scanning Electron Microscopy (SEM) and optical microscopy (OM) images, the samples were sequentially grinded with silicon carbide emery paper of grain sizes 400, 600, 1200 and P4000. Polishing was made with diamond polishing abrasives of 3 and 1 μm using appropriate polishing pads. The lubricant that was chosen to be used during the grinding and polishing steps was a mixture of glycerin and isopropyl alcohol 1:3 v/v, to avoid the risk of ignition posed by dry Mg powder and also to avoid the corrosion of the samples.
A solution of 10 mL HNO_3, 30 mL glacial acetic acid, 40 mL of water and 120 mL of ethanol was used to make the chemical polishing and to obtain OM images (BX60MF, Olympus Optical Co. Ltd. with a coupled OPTICAM camera) of the MgCa alloy microstructure.
Electrochemical and corrosion tests were carried out in 0.1 mol/L NaCl solution. A classical three electrode mounting was used to perform the former tests with the Mg samples as working electrode, an Ag/AgCl electrode as reference and a Pt grid as counter electrode.
Open circuit potential (OCP) measurements were taken during 24h to assure the stability of the corrosion potential of the samples necessary for the EIS (Electrochemical Impedance

Spectroscopy) experiments. These measurements were taken during 24h, the first one soon after the stabilization of the OCP and afterwards at an interval of 6 h between each measurement. The AC potential sign applied to the samples was 15 mV around the OCP and the acquisition rate was 7 points per decade. The frequency interval was from 0.01 Hz to 10^5 Hz.
The polarization curves of the alloys were taken after 3600 s of immersion and after 24h of immersion. The applied voltage ranged from -1.0 V below the OCP and 1.0 V above the OCP, at a scan rate of 1mV/s.
A PAR SI1287 potentionstat was employed to acquire the OCP and the polarization curves, which was coupled to a Solartron SI1260 frequency response analyzer during the EIS experiments.
An immersion test was carried out to evaluate the corrosion behavior of the MgCa and AZ91 alloys. This essay consisted in the immersion of the samples in the test solution for 30 min. In the procedure, little spots were marked on the surface of the samples with a microhardness tester (HMV, Shimadzu) so that the exact position of selected intermetallics could be traced back. SEM images (Inspect F50, FEI) of the same regions of the samples were taken before and after the immersion tests. The composition of the intermetallics and of the alloy phases were evaluated by EDS (Energy-Dispersive X-Ray Spectroscopy).
During the immersion tests, the solution volume used was such to maintain the ratio of $1cm^2$: 20 mL suggested by Zhang *et al.* (4) in their work with Mg-Zn alloys.

Results and Discussion

Table 1 shows the overall composition of the alloys. It shows that the composition of the MgCa alloy consists mainly of Mg and Ca (0.67 wt %) and that Al, Si and other elements are present as impurities. The AZ91 is composed mainly by Mg, Al (8.6388 wt %), Zn (0.6204 wt %) and Mn (0.1453 wt %) with Fe and Nb as impurities. The composition of the AZ91 alloy is similar to that found by Mathieu *et al.* (5).

Table 1 – Composition of the MgCa and AZ91 alloys

	Composition (wt %)	
Chemical Element	**MgCa**	**AZ91**
Ag	<0.0001	-
Al	0.030	8.6388
Be	-	< 0.0020
Ca	0.67	< 0.0020
Ce	0.0026	-

Cu	0.0045	< 0.0020
Fe	0.0044	0.0196
La	<0.0012	-
Mn	0.043	0.1453
Nb	-	0.0137
Ni	0.0067	< 0.0020
Pb	<0.0004	-
Si	0.024	< 0.0020
Sn	<0.0005	-
Zn	0.0024	0.6204
Zr	0.0050	< 0.0020

The microstructural characterization of the alloys was also evaluated by optical microscopy (OM) images, as shown in Figure 1(a), 1(b) and 1(c). These figures show, respectively, the OM images of the MgCa alloy after grinding and polishing (Figure 1(a)), of the MgCa alloy after grinding, polishing and etching (Figure 1(b)) and of the AZ91 alloy after grinding and polishing (Figure 1(c)).

It was possible to verify the presence of the α(Mg) phase, of the intermetallics CaMgSi and of the eutectic phase composed by the α(Mg) phase and the Mg_2Ca phase in the MgCa alloy, this latter phase mostly but not exclusively confined at the grain boundaries, as shown in Figure 1(a) and indicated by arrows. The darker spots in Figure 1(a) are the eutectic phase wherein some CaMgSi intermetallics are present. It is possible to infer that these intermetallics are cathodic in relation to the α(Mg) phase matrix, as shown in Figure 1(b) and indicated by arrows, because their complete dissolution is not observed after the etching procedure. It is also possible to infer from Figure 1(b) that the dissolution of the surrounding matrix due to galvanic coupling leads to the detachment of some intermetallics from the matrix. These images are very similar to those found by Mareci *et al.* (6) in their work with binary MgCa alloys. Kirkland *et al.* (7) found images similar to these and cited the presence of an interdentritic eutectic phase at the grain boundaries.

The AZ91 alloy (Figure 1(c)) is composed by the α(Mg) and the eutectic phase, this latter composed by the α(Mg) and the β($Mg_{17}Al_{12}$) phases, as explained by Mathieu *et al.* (5) in his work on the corrosion behavior of AZ91D alloys. Also evident is the presence of the Al and Mn intermetallics (MnAl). The eutectic phase appears as stains and the intermetallics as irregular shaped features, both of them are darker than the matrix, and are indicated by arrows

in the Figure. According to Song *et al.* (8), the irregular shaped hole at the top of the image in Figure 1(c) is likely attributed to the falling out of a brittle β($Mg_{17}Al_{12}$) particle.

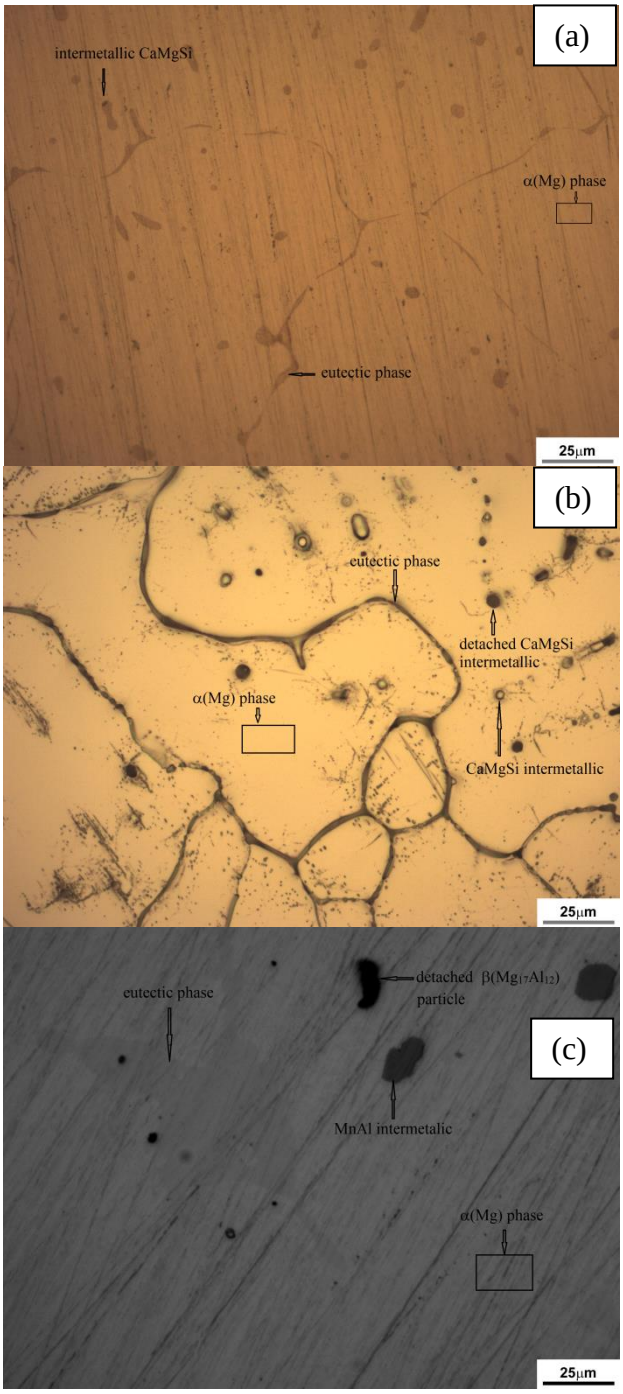

Figure 1 – (a) OM image of a MgCa alloy sample ground and polished. (b) OM image of a MgCa alloy sample ground, polished and etched. (c) OM image of an AZ91 alloy sample ground and polished

Figure 2 shows SEM images of selected areas of a sample of the MgCa alloy (Figure 2(a) and 2(c)) and of a sample of the AZ91 alloy (Figure 2(e)) after polishing. Whereas, Figures 2(b),

2(d) and 2(f) show the same regions presented in Figure 2(a), 2(c) and 2(e), respectively, after immersion in NaCl 0.1 mol/L for 30 minutes. In Figure 2(a), the spots 1 and 2 correspond to the intermetallic CaMgSi, the spot 3 to the eutectic phase and the selected area is the α(Mg) phase. In Figure 2(c), the spot 1 corresponds to the intermetallic CaMgSi and spot 2 to the eutectic phase. The approximate compositions of these constituents measured by EDS are shown in Table 2.

As already mentioned, the constituents of the MgCa alloy are the α(Mg) phase, the CaMgSi intermetallics and the eutectic phase composed by the α(Mg) phase and Mg_2Ca. The presence of Si in the composition of the alloy caused the formation of this intermetallic, in addition to the formation of the Mg_2Ca phase, this latter predicted by the binary phase diagram of this alloy. Salahshoor *et al*. (9) found similarities in the morphological structure in their study with a MgCa alloy containing 0.5 wt % Ca to those found in this work. Furthermore, Kirkland *et al.* (7) cited that the presence of the Mg_2Ca phase is typical for MgCa alloys to a composition of up to ~45 wt % Ca. In their work, it was shown that the presence of this second phase had a significant impact upon the measured anodic kinetics of pure Mg as shown by a shift in the anodic branches of the polarization curves towards significantly higher current densities with increasing Ca additions. In contrast, the corresponding cathodic branches were relatively unaffected by Ca additions. This result suggests, therefore, that Mg_2Ca is a more efficient anode than α(Mg).

The anodic behavior of the Mg_2Ca phase was proved by the results of the immersion tests in NaCl 0.1 mol/L. The approximate compositions of the constituents of MgCa alloy after immersion in NaCl 0.1 mol/L for 30 minutes, measured by EDS, are shown in Table 4. It is possible to verify an increase in the O content for all the selected points, indicating the formation of oxides/hydroxides. It is also possible to verify the dissolution of Mg into the solution, as proved by the diminishment of the Mg content in point 3 of Figure 2(a) and in the selected area of the same Figure.

It was possible to infer that corrosion of the surrounding areas of the intermetallic CaMgSi led to an increase in the oxygen content in these regions, as seen in the composition of the intermetallic characterized in spot 1 of Figure 2(b). The O content in this area went from 0.78 wt % (Table 2) to 17.62 wt % (Table 4), indicating the precipitation of $Mg(OH)_2$. Apparently the intermetallic itself did not suffer dissolution, as its composition hardly changed.

It was also possible to confirm the anodic behavior of the eutectic phase when compared to the matrix, due to the presence of the Mg_2Ca phase, by analyzing the results shown in Figure 2(b) and 2(d). The area under spot 3 in Figure 2(b) suffered severe corrosion, with the content of O increasing from 0 wt % (Table 2) to 8.38 wt % (Table 4). This result was also found in the area under spot 3 in Figure 2(d), in which the eutectic phase suffered severe dissolution.

The selected area in Figure 2(b) of the α(Mg) phase showed a higher content of O and the decrease in the Mg content, which diminished from 99.66 wt % to 93.54 wt %, indicating the formation of oxide/hydroxide. This points to a generalized corrosion of the matrix.

The constituents of the AZ91 alloy were found to be the α(Mg) phase, the eutectic composed by the α(Mg) and the β($Mg_{17}Al_{12}$) phases and the intermetallics composed of Al and Mn (MnAl). In Table 3, the chemical compositions of these constituents are shown. The spots 2 and 3 of Figure 2(e) were marked over the intermetallics (MnAl), whilst spots 4 and 6 correspond to the eutectic phase (Table 2). The selected area marked in Figure 2(e) corresponds to the α(Mg) phase.

The approximate compositions of the constituents of the AZ91 alloy after immersion in NaCl 0.1 mol/L for 30 minutes, determined by EDS, are shown in Table 5. The high contents of O

in spots 2 and 3 over the intermetallics are probably due to the corrosion of the surrounding matrix. In spots 4 and 6 of the eutectic phase, the corrosion might have happened more intensely in the α(Mg) phase, which is more anodic compared to the β($Mg_{17}Al_{12}$). The α(Mg) phase suffered corrosion forming oxides/hydroxides as proved by the increase in O determined by EDS. The accumulation of Na and Cl was higher in the regions of the intermetallics (MnAl).

Mathieu *et al.* (10) in his work of the main constituent phases of the AZ91 Mg alloy, found that the scale of nobility of its constituents was as follows: α(Mg) phase is less noble than the β($Mg_{17}Al_{12}$), which was less noble than the MnAl intermetallic. The E_{CORR} of these constituents were -1.43 V (SCE), -1.31 V (SCE) and -1.28 V (SCE), respectively, after 3 h of immersion in ASTM D1384 water. In his work, he measured the E_{CORR} of the α(Mg) phase with a content of 0.5 at % Zn and 5 at % Al, which is similar to the composition found in the selected area of Figure 2(e). The contents of these constituents in the selected area of the AZ91 alloy shown in Figure 2(e) are 0.51 at % Zn and 4.57 at % Al.

Finally, the general analysis of the micrographs presented in Figure 2 indicates a more intense corrosion process for the MgCa alloy.

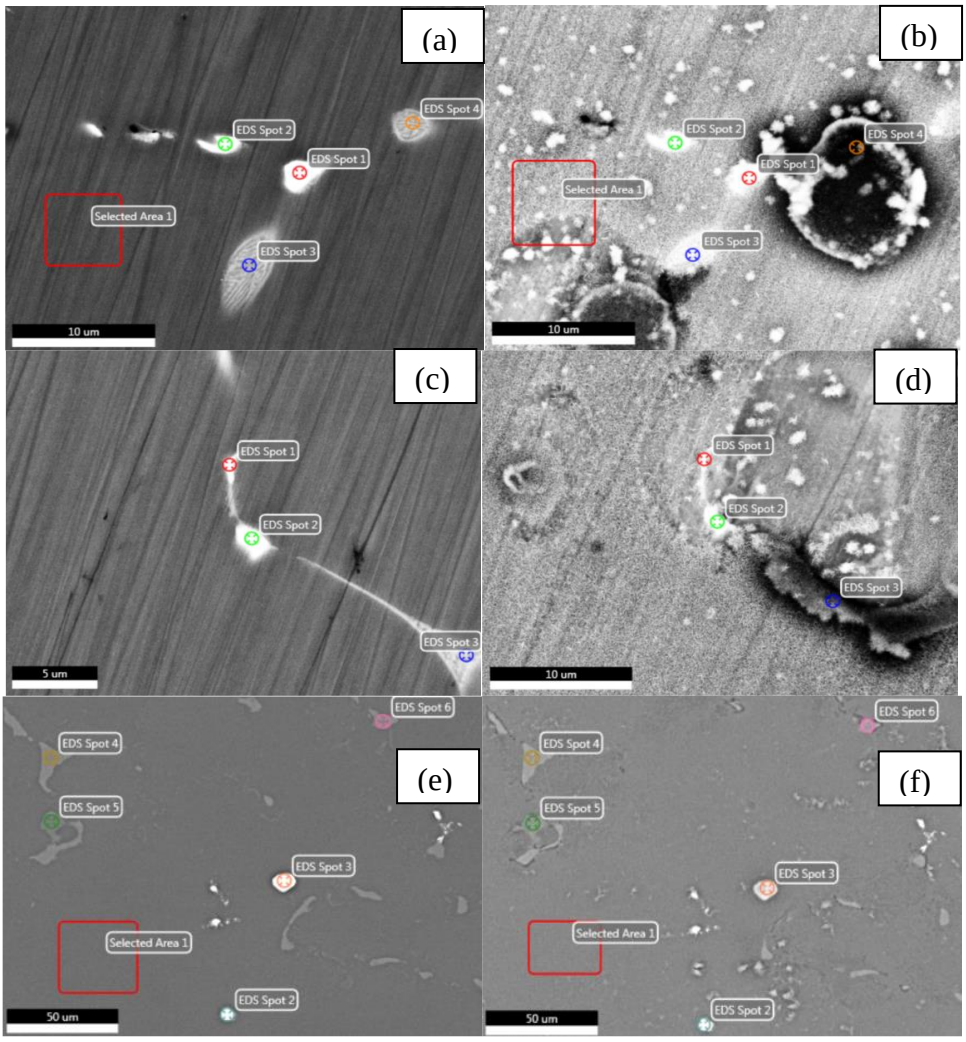

Figure 2 – (a), (c) SEM images of different regions of the MgCa alloy. (e) SEM images of a region of the AZ91 alloy. (b), (d) SEM images of the MgCa alloy after

immersion in NaCl 0.1 mol/L for 30 minutes, the regions are the same presented in (a) and (c), respectively. (f) SEM images of the MgCa alloy after immersion in NaCl 0.1 mol/L for 30 minutes, the region is the same presented in (e)

Table 2 – Selected points in Figure 2(a) and (c) and their weight percentage composition by chemical element as determined by EDS analysis

	Spot 1 - Figure 2(a)	Spot 2 - Figure 2(a)	Spot 3 – Figure 2(a)	Selected area 1 – Figure 2(a)	Spot 1 - Figure 2(c)	Spot 2 - Figure 2 (c)
Element	**Weight (%)**	**Weight (%)**	**Weight (%)**	**Weight (%)**	**Weight (%)**	**Weight (%)**
O	0.78	-	-	-	-	-
Mg	48.77	65.73	85.86	99.66	78.20	63.68
Si	18.57	13.67	-	-	8.85	14.40
Ca	31.88	20.59	13.38	0.34	12.47	21.93
Al	-	-	0.76	-	0.48	-

Table 3 – Selected points in Figure 2(e) and their weight percentage composition by chemical element as determined by EDS analysis

	Spot 2 - Figure 2(e)	Spot 3 - Figure 2(e)	Spot 4 – Figure 2(e)	Spot 6 - Figure 2 (e)	Selected area 1 – Figure 2(e)
Element	**Weight (%)**	**Weight (%)**	**Weight (%)**	**Weight (%)**	**Weight (%)**
O	2.63	2.48	-	-	1.04
Mg	1.51	1.18	58.92	60.37	92.45
Si	0.86	0.76	-	-	-
Al	40.01	40.11	37.15	36.33	5.02
Mn	54.99	55.46	-	-	-
Zn	-	-	3.93	3.23	1.35
Mo	-	-	-	0.07	0.13

Table 4 – Selected points in Figure 2(b) and (d) and their weight percentage composition by chemical element as determined by EDS analysis. Analysis performed after 30 min immersion in NaCl 0.1 mol/L

	Spot 1 - Figure 2(b)	Spot 2 - Figure 2(b)	Spot 3 – Figure 2(b)	Selected area 1 – Figure 2(b)	Spot 1 - Figure 2(d)	Spot 2 - Figure 2(d)

Element	Weight (%)	Weight (%)	Weight (%)	Weight (%)	Weight (%)	Weight (%)
O	17.62	9.32	8.38	6.17	11.62	16.24
Mg	46.39	60.14	79.54	93.54	73.04	55.38
Si	13.22	12.12	-	-	7.45	11.70
Ca	22.55	18.41	12.08	0.29	7.89	16.68
Al	0.22	-	-	-	-	-
Cl	-	-	-	-	-	-

Table 5 – Selected points in Figure 2(f) and their weight percentage composition by chemical element as determined by EDS analysis. Analysis performed after 30 min immersion in NaCl 0.1 mol/L

	Spot 2 - Figure 2(f)	Spot 3 - Figure 2(f)	Spot 4 – Figure 2(f)	Spot 6 - Figure 2(f)	Selected area 1 – Figure 2(f)
Element	**Weight (%)**	**Weight (%)**	**Weight (%)**	**Weight (%)**	**Weight (%)**
O	5.50	11.08	4.79	6.35	2.81
Mg	3.91	8.75	57.22	57.87	90.58
Si	0.91	0.57	-	-	-
Al	36.50	28.13	35.12	31.02	5.67
Mn	49.30	33.78	-	-	-
Zn	-	-	2.49	4.12	0.40
Na	3.19	8.80	0.00	0.00	0.00
Cl	0.69	3.88	0.37	0.64	0.44
Mo	-	-	-	-	0.10

Figure 3 shows the OCP of the MgCa and AZ91 alloys in NaCl 0.1 mol/L throughout the duration of the essay, which remained constant and stable during 24 h. The OCP of the AZ91 alloy was higher than that of the MgCa alloy, indicating that the former alloy is nobler than the latter. The OCP of the AZ91 after 24 h of immersion in NaCl 0.1 mol/L was -1.51 V (Ag/AgCl). The OCP of the MgCa after 24 h of immersion in NaCl 0.1 mol/L was -1.55 V (Ag/AgCl). Song *et al.* (8) found an OCP of approximately -1570 mV (SCE) for AZ91 in

NaCl 1 mol/L in his study of the corrosion behavior of Mg alloys. Daroonparvar *et al.* (11) in his work with a MgCa alloy with 1.0 wt % Ca found a value of OCP of -1628 mV (SCE) for this alloy in NaCl 3.5 wt %.

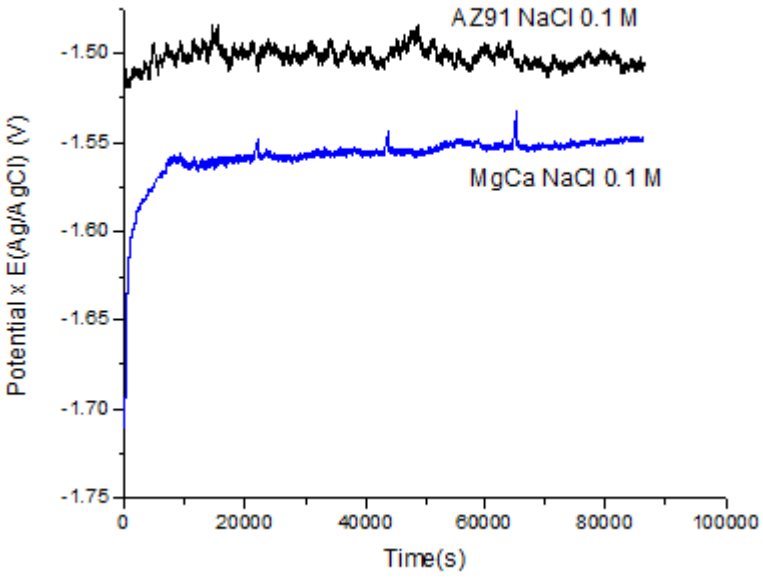

Figure 3 – OCP of the MgCa and AZ91 alloys immersed in NaCl 0.1 mol/L throughout the duration of the essay (24h)

Figures 4(a) and 4(b) contain, respectively, the Nyquist and the Bode phase angle diagrams of the MgCa alloy in NaCl 0.1 mol/L solution. The data were taken during 24 h. The first measurement was performed after 5000 s (1.39 h) of stabilization of the OCP. The remaining four experiments were carried out after 6, 12, 18 and 24 h of immersion of the sample in the test solution.

The impedance data taken after 1.39 h of immersion show two capacitive and one inductive loop. The other EIS data show only one capacitive and one inductive loop. Crimu *et al.*(12) in their study about degradation characteristics of a MgCa alloy with 0.81 wt % Ca in NaCl 0.9 wt % found similar results, except for the data after 1 h, at which they found only one capacitive loop. The same diminishment in the dimension of the overall impedance during time evolution was observed by Crimu *et al.* (12). This is an indication that the corrosion resistance of the alloy decreases with time in this medium. In addition, the preliminary analysis of the diagrams indicates that, as time elapses, the high frequency loop disappears, as only the capacitive loop at medium frequencies remains for longer test times.

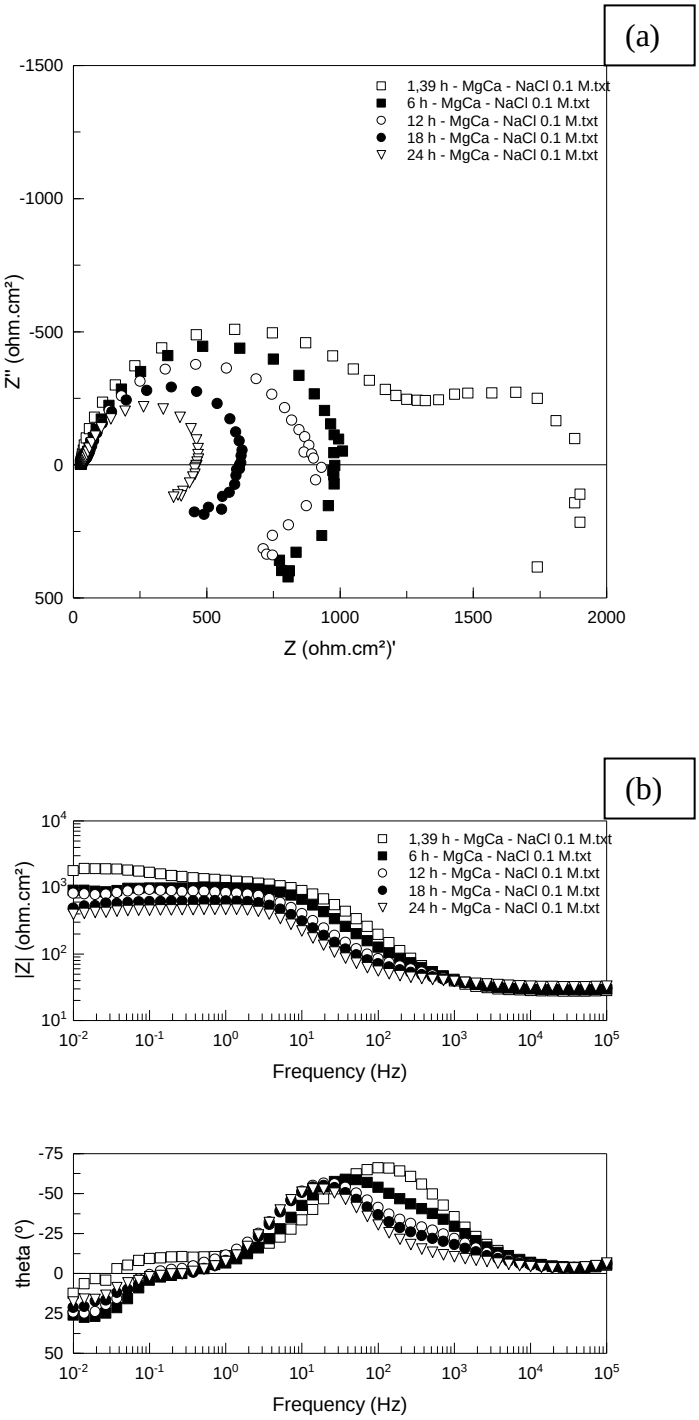

Figure 4 – EIS diagrams of the MgCa alloy immersed in NaCl 0.1 mol/L throughout the time of the essay (24h); (a) Nyquist diagram, (b) Bode phase angle diagrams

Figures 5(a) and 5(b) display, respectively, the Nyquist and the Bode phase angle diagrams of the AZ91 alloy in NaCl 0.1 mol/L solution. The sequence of experiments was the same described for the MgCa alloy. During the whole test period the impedance data showed only

one capacitive and one inductive loop. Song *et al.* (8) in their study about degradation characteristics of the AZ91 alloy in NaCl 1 mol/L found similar results. It is possible to see a diminishment in the dimension of the overall impedance with immersion time, indicating a decreasing of the corrosion resistance. However, overall the impedance modulus of the AZ91 alloy was higher than that of the MgCa alloy indicating better corrosion resistance, which is in accordance with the immersion tests previously discussed.

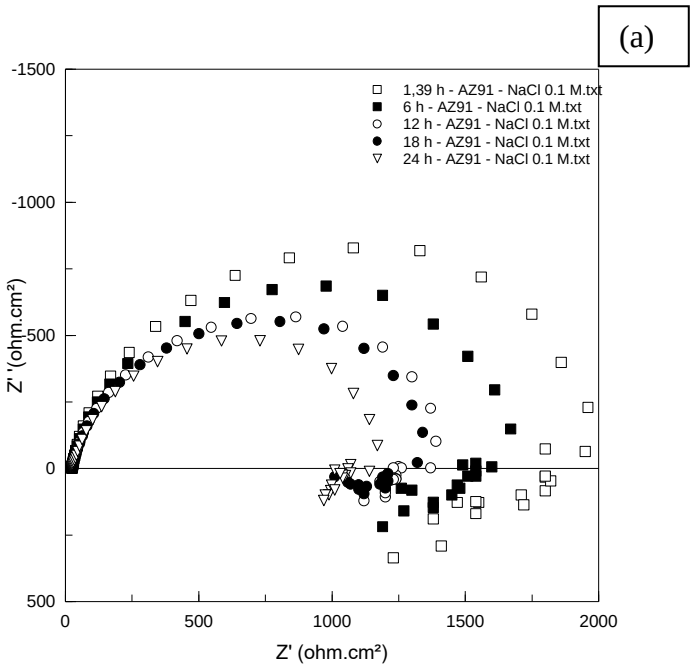

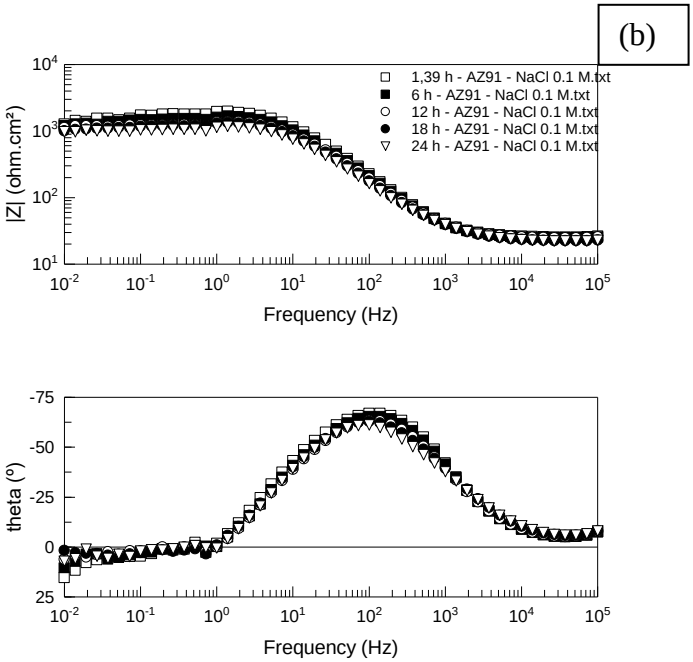

Figure 5 – EIS diagrams of the AZ91 alloy immersed in NaCl 0.1 mol/L throughout the time of the essay (24h); (a) Nyquist diagram, (b) Bode phase angle diagrams

The polarization curves in Figure 6 show the essay of the alloys in NaCl 0.1 mol/L after 1 h immersion in the test electrolyte. The data were acquired from -1.0 V below the OCP until 1.0 V above this value at a scan rate of 1 mV/s and 0.001 V/step. The corrosion potential found was approximately -1.42 V (Ag/AgCl) for AZ91 and -1.56 V (Ag/AgCl) for MgCa, which are in good agreement with the OCP. The curves also show that both the anodic and the cathodic process is activation controlled. Moreover the cathodic branch is slightly more depolarized for the AZ91 alloy, this might be a consequence of the cathodic nature of the eutectic phase and the intermetallics when compared to the alloy matrix, providing larger areas for the reduction reaction.

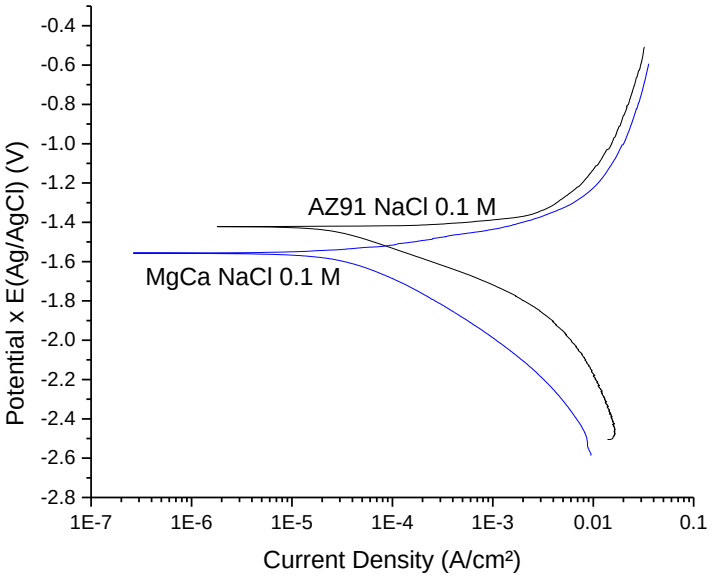

Figure 6 – Polarization curves of MgCa and AZ91 alloys in NaCl 0.1 mol/L after stabilization of OCP during 3600 s

The polarization curves in Figure 7 show the essay of the alloys in NaCl 0.1 mol/L after 24h immersion, the conditions for data acquisition were the same previously described. The corrosion potential found was approximately -1.38 V (Ag/AgCl) for AZ91 and -1.41 V (Ag/AgCl) for MgCa. At this condition the polarization curves were quite similar and there was not much difference in the anodic and cathodic branches for both alloys.

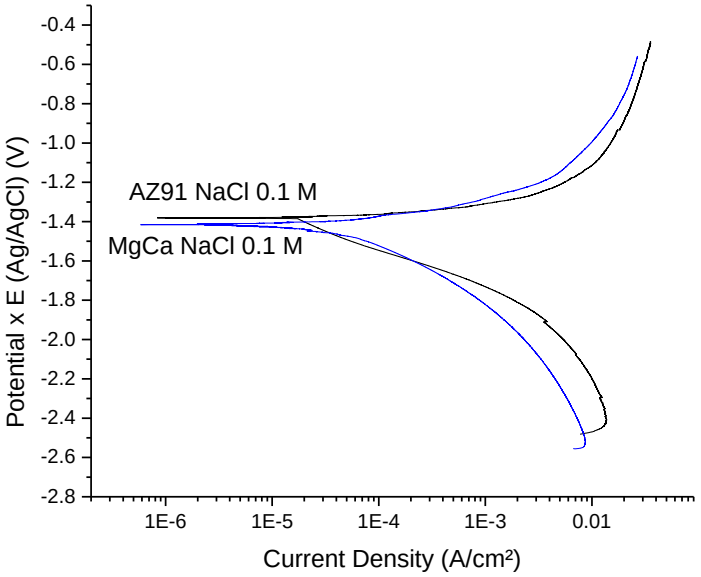

Figure 7 – Polarization curves of MgCa and AZ91 alloys in NaCl 0.1 mol/L after stabilization of OCP during 24 h

The current densities (i_{CORR}) of the alloys were calculated by Tafel extrapolation of the cathodic branch. This was feasible for all the curves because they showed a linear region, indicating an activation control of the interfacial process. The beginning of the Tafel region was considered to be 0.05 V (Ag/AgCl) bellow the E_{CORR}. Equation 1 was used to calculate the corrosion rate of the alloys in NaCl 0.1 mol/L.

Equation 1: $$i_{CORR} = V_{CORR} \times \frac{96500 \frac{C}{mol}}{Eq_{METAL}}$$

E_{qMetal} is the value of the atomic weight of Mg (24.305 g/mol) divided by the number of electrons of its oxidation reaction: 2. The necessary conversions were made to obtain the corrosion rates in different unities, like g/(cm² s) and mg/(cm² year). The value of E_{CORR} was determined from the polarizations curves. The thickness loss (TL) of the alloys in the different conditions was calculated by Equation 2.

Equation 2: $$TL = \frac{v_{CORR}}{\rho_{METAL}}$$

In Equation 2, ρ_{Metal}, is the density of Mg (1.739 g/cm³). The measurement unity of TL is mm/year. The data in Table 6 show that the corrosion rate of MgCa is higher than that of the AZ91 alloy for both periods of stabilization of the OCP (3600 s and 24 h). Singh *et al.* (13) in his work with Mg alloys in NaCl 3.5 wt % found a I_{CORR} of 25.5 x 10^{-6} A/cm² for AZ91, comparable to the value found in this work of 24.0x10^{-6} A/cm². Wu *et al.* (14) found a I_{CORR} of 22.84x10^{-5} A/cm² in a study of the corrosion of a MgCa alloy containing 2.05 wt % of Ca in NaCl 3.5 wt %, this was about 5-6 times higher than that determined in the present work. However, the Ca content in Wu *et al*. (14) alloy was about 3.5 higher than that of the MgCa employed in the present investigation; in addition their electrolyte was more aggressive.
The results of the Tafel extrapolation methodology also indicated that both alloys showed a decrease in the corrosion rates after 24 h in NaCl 0.1 mol/L. This is not in accordance with the EIS measurements that showed a continuous decrease of the impedance with immersion time, indicating that, for both alloys, the corrosion process is not being hindered by the deposition of corrosion products. It is hypothesized that the precipitation of corrosion products during the cathodic polarization step may have affected the results. In order to verify this hypothesis, experiments using different electrodes to acquire the cathodic and anodic branches will be performed.

Table 6 – Corrosion rates expressed in different unities and the E_{CORR} of the AZ91 and MgCa alloys immersed in NaCl 0.1 mol/L

Time of stabilization of the OCP	**3600 s**		**24 h**	
Alloy	**MgCa**	**AZ91**	**MgCa**	**AZ91**
i_{corr} (A/cm²)	3.93x10^{-05}	2.40x10^{-05}	3.41x10^{-05}	1.25x10^{-05}
E_{corr} (V/Ag/AgCl)	-1.56	-1.42	-1.41	-1.38

v_{corr} (g/(cm² s))	$4.95x10^{-09}$	$3.02x10^{-09}$	$4.29x10^{-09}$	$1.57x10^{-09}$
v_{corr} (mg/(cm² year))	$1.56x10^{02}$	$9.53x10^{01}$	$1.35x10^{02}$	$4.96x10^{01}$
TL (mm/year)	$8.99x10^{-01}$	$5.48x10^{-01}$	$7.79x10^{-01}$	$2.86x10^{-01}$

Conclusions

The morphological characterization of the MgCa alloy showed that this alloy is composed by three different phases: α(Mg), a eutectic phase composed by α(Mg) and Mg_2Ca and an intermetallic phase composed of Ca, Si and Mg (CaMgSi intermetallic). The morphological characterization of the AZ91 alloy showed that this alloy is composed by three different phases: α(Mg), a eutectic phase composed by α(Mg) and β($Mg_{17}Al_{12}$) phase and an intermetallic phase composed of Al and Mn (MnAl intermetallic).
The SEM images and EDS analyses showed that the Mg_2Ca phase, which is confined inside the eutectic phase, is more anodic than the other constituents of the MgCa alloy. This phase suffered severe dissolution after 30 min of immersion in NaCl 0.1 mol/L. The β($Mg_{17}Al_{12}$), which is also confined within the eutectic phase, suffered less corrosion than the α(Mg) phase of the AZ91. The results also showed that the eutectic phase of the MgCa alloy is more susceptible to corrosion than the α(Mg), whereas, for the AZ91 alloy the eutectic phase is nobler than α(Mg) matrix. The different behaviors can be ascribed to the nature of the intermetallics within each of these eutectic phases.
It was possible to verify the stability of the OCP of the alloys in NaCl 0.1 mol/L during 24 h. The OCP of the MgCa alloy was lower than the OCP of the AZ91 alloy, which suggests that MgCa is less noble than the AZ91 alloy. This was confirmed by the results of the EIS measurements that showed lower impedance modulus for the MgCa alloy. For both alloys the impedance modulus decreased with immersion time, indicating increased interfacial corrosion activity.
The polarization curves showed a higher value of current density for the MgCa alloy in NaCl 0.1 mol/L compared to that of the AZ91 alloy independently of the immersion time, which was 24h in the present investigation.

References

(1) Chen Y, Xu Z, Smith C, Sankar J. Recent advances on the development of magnesium alloys for biodegradable implants. **Acta Biomaterialia.** (2014) 10: 4561 – 4573.

(2) Choudhary L, Raman RKS. Magnesium alloys as body implants: Fracture mechanism under dynamic and static loadings in a physiological environment. ***Acta Biomaterialia.*** (2012) 8: 916 – 923.

(3) Witte F, Hort N, Vogt C, Cohen S, Kainer KU *et al.*. Degradable biomaterials based on magnesium corrosion. **Current Opinion in Solid State and Materials Science.** (2008) 12: 63 – 72.

(4) Zhang S, Zhang X, Zhao C, Li J, Song Y *et al.*. Research on an Mg–Zn alloy as a degradable biomaterial. **Acta Biomaterialia.** (2010) 6: 626 - 640.

(5) Mathieu S, Rapin C, Hazan J, Steinmetz P. Corrosion behaviour of high pressure die-cast and semi-solid cast AZ91D alloys. **Corrosion Science.** (2002) 44: 2737 – 2756.

(6) Mareci D, Bolat G, Izquierdo J, Crimu C, Munteanu C *et al.*. Electrochemical characteristics of bioresorbable binary MgCa alloys in Ringer's solution: Revealing the impact of local pH distributions during *in-vitro* dissolution. **Materials Science and Engineering C.** (2016) 60: 402 – 410.

(7) Kirkland NT, Birbilis N, Walker J, Woodfield T, Dias GJ *et al.*. *In-vitro* dissolution of magnesium–calcium binary alloys: Clarifying the unique role of calcium additions in bioresorbable magnesium implant alloys. **Journal of Biomedical Materials Research B: Applied Biomaterials.** (2010) 95B(1): 91 – 100.

(8) Song G, Atrens A, Wu X, Zhang B. Corrosion behaviour of AZ21, AZ501 and AZ91 in sodium chloride. **Corrosion Science.** (1998) 40(10): 1769 – 1791.

(9) Salahshoor M, Guo Y. Biodegradable Orthopedic Magnesium-Calcium (MgCa) Alloys, Processing, and Corrosion Performance. **Materials.** (2012) 5: 135 – 155.

(10) Mathieu S, Rapin C, Steinmetz J, Steinmetz P. A corrosion study of the main constituent phases of AZ91 magnesium alloys. **Corrosion Science.** (2003) 45: 2741-2755.

(11) Daroonparvar M, Yajid MAM, Yusof NM, Bakhsheshi-Rad HR. Preparation and corrosion resistance of a nanocomposite plasma electrolytic oxidation coating on Mg-1%Ca alloy formed in aluminate electrolyte containing titania nano-additives. **Journal of Alloys and Compounds.** (2016) 688: 841 – 857.

(12) Crimu C, Bolat G, Munteanu C, Mareci D. Degradation characteristics of Mg0.8Ca in saline solution with and without albumin protein investigated by electrochemical impedance spectroscopy. **Materials and Corrosion.** (2015) 66(7): 649 – 655.

(13) Singh IB, Singh M, Das S. A comparative corrosion behavior of Mg, AZ31 and AZ91 alloys in 3.5% NaCl solution. **Journal of Magnesium and alloys.** (2015) 3: 142 – 148.

(14) Wu P-p, Xu F-j, Deng K-k, Han F-y, Zhang Z-z *et al.*. Effect of extrusion on corrosion properties of Mg-2Ca-χAl (χ = 0, 2, 3, 5) alloys. **Corrosion Science.** (2017) 127: 280 – 290.